Steel and Composite Structures, *Vol. 33, No. 3* (*2019*) *333-346*
DOI: https://doi.org/10.12989/scs.2019.33.3.333

Factors governing dynamic response of steel-foam ceramic protected RC slabs under blast loads

Xiaomeng Hou*[1,2], Kunyu Liu [1,2a], Shaojun Cao [1,2b] and Qin Rong [1,3c]

[1] *Key Lab of Structures Dynamic Behavior and Control of the Ministry of Education*, *Harbin Institute of Technology*, *Harbin*, *150090*, *China*
[2] *Key Lab of the Smart Prevention and Mitigation of Civil Engineering Disasters of the Ministry of Industry and Information Technology*, *Harbin Institute of Technology*, *Harbin*, *150090*, *China*
[3] *School of Architecture and Civil Engineering*, *Harbin University of Science and Technology*, *Harbin 150080*, *China*

(*Received October 26, 2018, Revised October 6, 2019, Accepted October 21, 2019*)

Abstract. Foam ceramic materials contribute to the explosion effect weakening on concrete structures, due to the corresponding excellent energy absorption ability. The blast resistance of concrete members could be improved through steel-foam ceramics as protective cladding layers. An approach for the modeling of dynamic response of steel-foam ceramic protected reinforced concrete (Steel-FC-RC) slabs under blast loading was presented with the LS-DYNA software. The orthogonal analysis (five factors with five levels) under three degrees of blast loads was conducted. The influence rankings and trend laws were further analyzed. The dynamic displacement of the slab bottom was significantly reduced by increasing the thickness of steel plate, foam ceramic and RC slab, while the displacement decreased slightly as the steel yield strength and the compressive strength of concrete increased. However, the optimized efficiency of blast resistance decreases with factors increase to higher level. Moreover, an efficient design method was reported based on the orthogonal analysis.

Keywords: composite slabs; dynamic analysis; structural design; numerical analysis; sandwich composite

1. Introduction

In recent years, frequently-occurred accidents such as explosion (Hao *et al.* 2016) and fire (Abid *et al.* 2019, Hou *et al.* 2019) have been caused serious damage on structures. In order to analyze the dynamic response under dynamic loads, the strain rate effect of material is also needed to be considered. The Split Hopkinson Pressure Bar (SHPB) experiments on concrete were conducted by Chen *et al.* (2016, 2017), Shi and Chen (2018). The results revealed that concrete is a strain rate sensitive material.

In addition to use better performance steel and concrete (Hou *et al.* 2018a), the set-up of sacrificial layers is also one of the ways to improve the blast-resistant capability and attenuate the explosive shock (Codina *et al.* 2017). Foam material offers energy-absorption and overpressure-weaken properties (Guzas and Earls 2010, Jing *et al.* 2013, Liang *et al.* 2017, Rashad and Yang 2018). Besides, metal foam (Hanssen *et al.* 2002, Wu *et al.* 2011, Xia *et al.* 2016), polymeric foam (Langdon *et al.* 2012, Ousji *et al.* 2016, Chuda-Kowalska and Garstecki 2016, Dear *et al.* 2017), syntactic foam (Pham *et al.* 2018) as well as foam ceramic (Wei *et al.* 2011, Ye *et al.* 2018) were used as cladding core, attenuation layer or barrier device to against blast, impact and other dynamic loads.

Foam ceramic is a lightweight, energy-absorption porous material, displaying excellent high temperature resistance, thermal shock resistance (Zake-Tiluga *et al.* 2015) as well as good chemical stability (Li *et al.* 2008). The results of gas explosion experiment and simulation also proved that foam ceramics could consume a kinetic energy portion of the explosion by deformation as well as weaken the maximum overpressure caused by the blast (Nie *et al.* 2011, Zhang *et al.* 2011).

Due to the difference in raw materials and porosities, some kinds of foam ceramics are of lower strength and stiffness than foam metal materials, such as aluminum foam (Mehr *et al.* 2016). However, aluminum foam materials cannot work well at approximately 200°C or more, due to the yield strength sharp decrease (Mondal *et al.* 2012). In addition, aluminum is easy to be corroded in complex chemical environments, such as acid or alkali environments, while the foams are of worse chemical stability compared to the chemical stability of few pores, due to the higher specific surface areas being exposed to the aggressive media. Therefore, compared to the aluminum foam materials, the foam ceramic displayed significantly higher temperature resistance and more excellent chemical stability. With the development of processing and the improvement of ductility, the foam ceramic is suitable for applications in protection engineering, as well as for comparisons to metal foams.

To test the dynamic compression properties of clay foam ceramics, the SHPB experiments were conducted under different strain rates (50 s^{-1}~180 s^{-1}) by Luo (2011) and Li *et*

*Corresponding author, Ph.D.,
E-mail: houxiaomeng@gmail.com
[a] Master
[b] Ph.D. Student
[c] Ph.D., E-mail: hitrongqin@126.com

ISSN: 1229-9367 (Print), 1598-6233 (Online)

Table 1 Comparison of material parameters of foam ceramic, normal concrete and steel

Material	Density (g/cm^3)	Modulus of elasticity (GPa)	Compressive strength (MPa)	Allowable working temperature (°C)
Foam ceramic	0.5~0.95	0.1~8	0.5~80	1000~2000
Normal concrete (Kodur 2014)	2.4	30~35	10~50	300~350
Steel	7.8~7.9	200	325~440	200~300

al. (2013). This demonstrated that the closed-cell foam ceramics produced strain rate increase effects. The strength under dynamic load, such as blast load, was twice the strength under quasi-static load. Moreover, the results demonstrated that the ideal energy absorption efficiency of closed-cell foam ceramics increased as the porosity increased. Furthermore, this type of clay closed-cell foam was set as the attenuation layer of underground civil defense and a large-scale explosion test was performed to verify the corresponding decompression capacity by Ye *et al.* (2018).

The material parameters of foam ceramics, normal concrete and steel are presented in Table 1. Based on the properties of each material, a new type of steel-foam ceramic protected reinforcement concrete (Steel-FC-RC) slab was presented. Foam ceramics especially with closed-cell have smaller modulus of elasticity, higher temperature resistance, and relatively high strength. Subsequently, foam ceramics could be used for sacrificial layers, in order to absorb portions of kinetic energy of blasts through conversion into deformation energy. Steels, having high strength and high modulus of elasticity, are installed outside the sacrificial layers to optimize the ductility of foam ceramics, as well as to enhance the rigidity of slabs and reflect portions of the shock waves of explosions. Reinforced concrete was used as the main structural layer of the slabs to sustain the dead and live loads of the structure.

Based on the finite element analysis (FEA) software LSDYNA, the dynamic response of Steel-FC-RC slabs under blast load were analyzed. The parametric analysis involved of thickness of each layer, the compressive strength of concrete, the yield strength of the steel, the foam ceramic porosity, the charge quantity and the explosion distance. These were studied in order to provide a reference for Steel-FC-RC blast-resistant slab design for protection engineering applications.

2. FEA model

Based on LS-DYNA, a numerical model of Steel-FC-RC two-way slabs was established. The SOLID164 element was used for steel plates, foam ceramics and concrete, while the BEAM161 element was used for steel bars (LS-DYNA 2006).

2.1 Foam ceramic

Clay foam ceramic is a closed-cell porous material, proved to have high energy absorption efficiency and

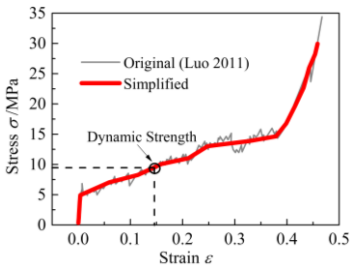

Fig. 1 Original and simplified stress-strain curves of clay foam ceramic

relatively high strength under high strain rates (Luo 2011). The numerical material model of clay foam ceramic was Crushable-Foam, which was used to simulate foam materials under dynamic loads, such as impacts and blasts, and proved to be reliable (Pinnoji *et al.* 2010, Krundaeva *et al*. 2016).

Based on the SHPB compressive experiment results of clay foam ceramics by Luo (2011) and Li *et al.* (2013), the simplified stress-strain curve was adopted (Fig. 1), to ensure the accuracy and efficiency of calculations. The strengths of materials presenting strain rate increase effect under dynamic loads, such as impacts and blasts, were higher than under quasi-static loads. In order to consider the strain-rate increase effect of clay foam ceramic, the maximum stress value of 9.41 MPa under the highest strain rate of 180 s^{-1} was selected (Luo 2011). The parameters of foam ceramic of the basic event are presented in Table 2.

2.2 Concrete

To consider the influence of strain rate (Hou *et al.* 2018b, c), the CSCM-Concrete (MAT-159) material model was adopted to represent the normal concrete under dynamic loading. The plastic surface yield function was defined in LS-DYNA as follows (Murray *et al.* 2007)

$$f(I_1, J_2, J_3) = J_2 - R^2 F_f^2 F_c \quad (1)$$

F_f is the shear failure surface function, related to the first invariant of shear tensor I1; F_c is the cap hardening surface function, related to I_1 and the cap hardening parameter;

Table 2 Values of material parameters of foam ceramic

Parameter	Density (kg/m^3)	Modulus of elasticity (MPa)	Poisson ratio	Stress-strain curve
Value	930	1192	0.114	Fig. 1

Table 3 Values of material parameters of concrete

Parameter	Density (kg/m^3)	Initial imperfection	Compressive strength (MPa)	Aggregate size (mm)
Value	2400	Without consideration	40	19

R is the Rubin three-invariant reduction factor, related to the third invariant of shear deviatoric stress tensor J_3; the Viscoplastic algorithm was adopted at each time step due to the strain rate increase effects of concrete. The parameters of concrete of the basic event are presented in Table 3.

2.3 Steel plates and bars

The steel plate and steel bars were simulated with the Plastic-Kinematic model, considering the strain-rate effect and isotropic, kinematic hardening plasticity. The hardening yield stress is defined as follows (LS-DYNA 2006)

$$\sigma_{SR} = \left[1 + \left(\frac{\dot{\varepsilon}}{C}\right)^{\frac{1}{P}}\right](\sigma_0 + \beta E_P \varepsilon_P^{eff}) \tag{2}$$

C and *P* are two strain rate parameters, $\dot{\varepsilon}$ is strain rate, ε_P^{eff} is the effective plastic strain, β is the hardening parameter, and E_P is the hardening modulus. The parameters of steel plates and bars are presented in Table 4 (Zhou *et al*. 2017).

2.4 Contacts definition

In order to ensure adequate bonding strength between each layer, the polyurethane (PU) adhesive was adopted to bond each layer (Silva *et al.* 2010). The failure of the PU adhesive was governed as follows

$$(\frac{\sigma_n}{NFLS})^2 + (\frac{\sigma_s}{SFLS})^2 \geq 1 \tag{3}$$

σ_n is the normal stress and *NFLS* is the limit normal stress. σ_s is the shear stress and *SFLS* is the limit shear stress. The contacts were defined by Automatic-Surface-To-Surface-Tiebreak. In this paper, SV8002 PU adhesive was used, which performs good adhesive properties on wood, metal and rigid foam. The limit normal stress of SV8002 is 7.6 MPa and the limit shear stress is 9.1 MPa (Luo 2015).

According to Xu and Lu (2013), during the blast loading phase, the slip effect between concrete and reinforcement is little. Although the "slip" may affect the displacement responses after the RC member reach its peak response, perfect-bond model was also adopted by many previous researchers to simplify the numerical models. (Jayasooriya *et al*. 2014, Castedo *et al.* 2015, Foglar *et al.* 2017). Thus, the contacts among the reinforcement bars and concrete were assumed as shared nodes and the relative slippage effects were ignored.

2.5 Blast loads

Two different blast load simulation methods mainly exist: ALE and ConWep. The ALE method required the building of an explosive material model and its possible expansion space through Eulerian meshing, while the main structures were built through Lagrangian meshing. Through the addition of ALE keywords to control the fluid-structure coupling, the blast wave effect on the structure could be simulated. The ConWep method was adopted to simulate the air blast loads in LS-DYNA more efficiently by using keyword Load-Blast-Enhanced.

3. Validations of FEA modelt

Since there is a lack of air blast experiments of foam ceramics currently, a two-step validation of FEA model was presented. The material model verifications of foam ceramic and concrete were based on the underground explosion test carried by Ye *et al*. (2018). Through the aluminum foam consideration, the same properties of porousness and energy-absorption effects of foam ceramic were demonstrated. The foam was a feasible material to validate the air blast model based on the air blast experiments conducted by Zhu *et al*. (2009).

3.1 Material model verification

Compared to the large-scale underground explosion test results (Ye *et al.* 2018), the material models of closed-cell foam ceramic and concrete were verified through the ALE method, the sketch of the test and the 1/4 FEA model are presented in Fig. 2. Charge weight of TNT was 4.75 kg, which was buried in the 250 mm thick overlaying soil. Below the charge was a 300 mm thick RC anti-penetration layer. The compressive strength was 40 MPa, while the yield strength of the reinforcement bars was 400 MPa. The

Table 4 Values of material parameters of steel bars

Parameter	Density (kg/m^3)	Poisson ratio	Modulus of elasticity (MPa)	Yield strength (MPa)	
Value	7830	0.28	2.0×10^5	Bars	Plates
				400	235
Parameter	Hardening parameter β	Strain rate parameter *C*	Strain rate parameter *P*	Failure strain	
Value	0	40	5	0.20	

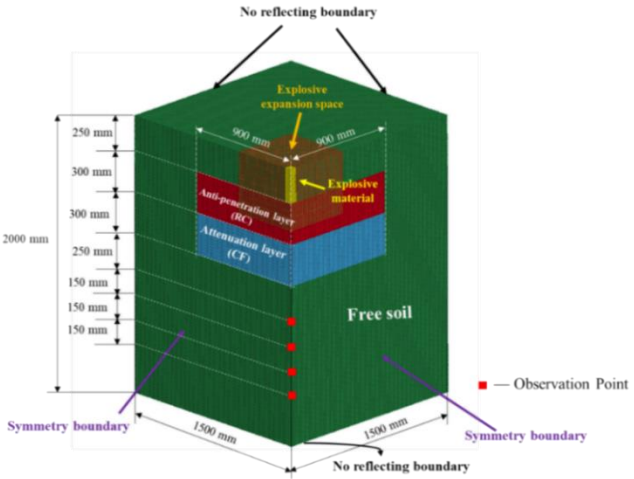

Fig. 2 Sketch of experiment and FEA model

reinforcement with 10 mm diameter and 20 cm × 20 cm mesh size were placed in the 1/3 and 2/3 height of the concrete slab. The bottom is the foam ceramic distribution layer, and the thickness is 30 cm. The sensors buried in the observation points in the soil were used to record the overpressure time-history (Fig. 1).

No reflecting boundary was set in the asymmetrical sides and the bottom, while the normal constraint boundary was set at the symmetry sides. The material models as well as the parameters of concrete and foam ceramic were the same to the parameters previously described. The material model of soil was Soil-and-Foam (Mat-005), while the explosive material was selected as the High-Explosive-Burn (Mat-008). The equation of state was EOS-JWL (Hafizi *et al*. 2017). In addition, the keyword Add-Erosion was used to control the excessive deformity of the materials.

The comparison of element failure patterns between FEA and experiment is presented Fig. 3, while the overpressure time histories at various underground depths are presented in Fig. 4.

According to the comparison, the failure patterns of FEA were similar to the experiment. The differences of underground depth overpressure between FEA and

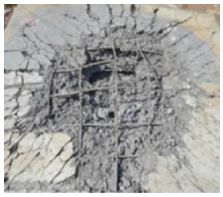

(a) Concrete of experiment

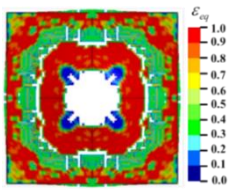

(b) Concrete of FEA

(c) Foam ceramic of experiment

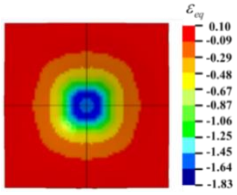

(d) Foam ceramic of FEA

Fig. 3 Failure patterns of experiment and FEA

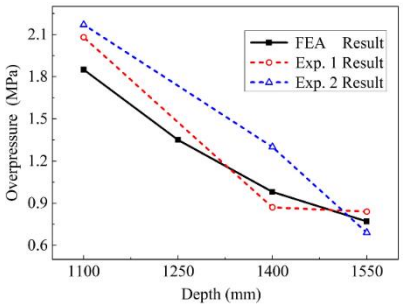

Fig. 4 Overpressure at different underground depth

experiments were less than 15%. Thus, the material models of concrete and foam ceramic are reliable for the following analysis.

3.2 Air blast verification

Based on the experiments of foam aluminum RC slabs (Zhu *et al*. 2009), the dimensions of foam aluminum-RC slabs are presented in Fig. 5. The stress-strain curve and material parameters of foam aluminum are presented in Fig. 6 and Table 5 (CYMAT 2008). The compressive strength of concrete was input as 32 MPa, while the yield strength of

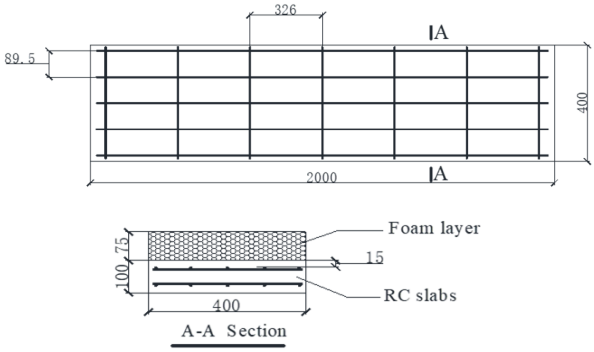

Fig. 5 Dimensions of foam aluminum-reinforced concrete slabs (mm)

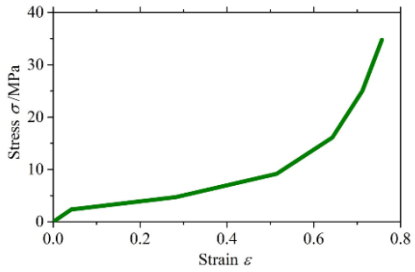

Fig. 6 Stress-strain curve of aluminum foam

Table 5 Values of material parameters of Aluminum foam

Parameter	Density (kg/m^3)	Modulus of elasticity (MPa)	Poisson ratio	Stress-strain curve
Value	400	500	0.19	Fig. 6

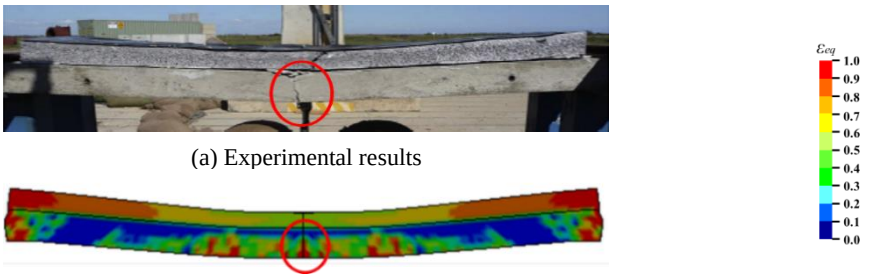

(a) Experimental results

(b) Simulation results

Fig. 7 Comparison of test results with simulation results of Event III

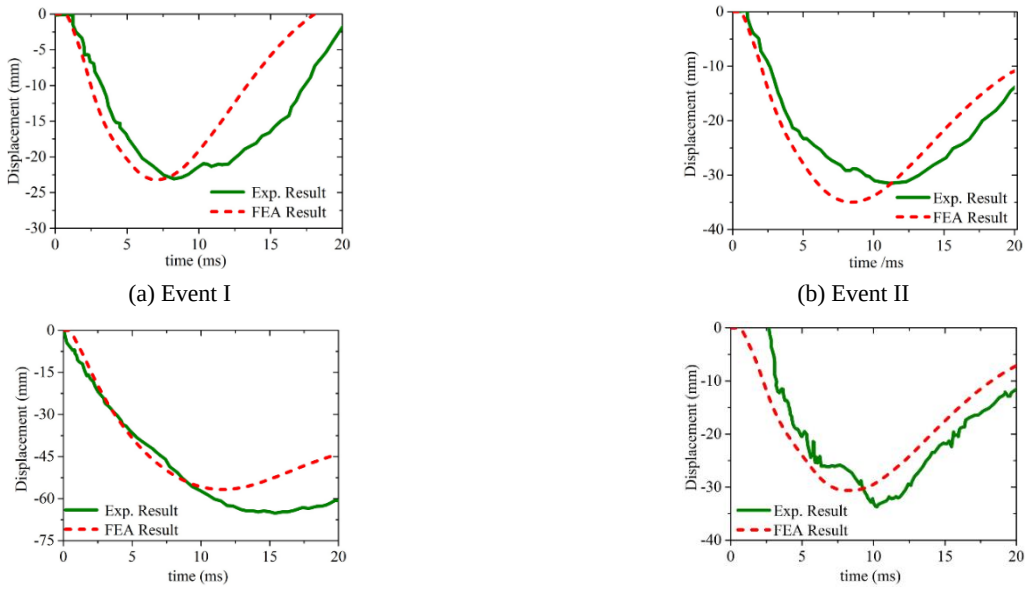

(a) Event I

(b) Event II

(c) Event III

(d) Event IV

Fig. 8 Displacement time history curve of central RC slab bottom

the reinforcement bars was 500 MPa. The charge was set above the center of the slabs, while the explosion distances were 1500 mm, 1250 mm and 1000 mm, marked as Events I, II and III. Also, the RC slabs without aluminum foam were set as a control group marked as Event IV. The corresponding explosion distance was 1500 mm.

According to the experiments, the boundary conditions of the long sides were set as free, while the edges of short sides were set as simply supported. The aluminum foam and the other materials were modeled with reference to the aforementioned parameters. The contact between each layer and the parameters were the same as the parameters described in section 2.4. In addition, the ConWep method was adopted to define the blast loads.

Through the consideration of Event III as an example, the effective plastic strain results of the numerical simulation and the experiment results were compared, as presented in Fig. 7. It could be observed from Fig. 7 that dynamic deformation response resemblances of the foam layers occurred, while the FEA results simulated the similar tensile damages near the mid-span of the RC layer. This revealed a good agreement between the finite element and experimental results.

Compared to the experiment results, the numerical results of the displacement curves of the slab bottom centers are illustrated in Fig. 8, while the maximum displacements

Table 6 Comparison of tested and calculated displacements of central point of slabs

Event	Charge weight C /g	Standoff distance R /mm	Foam thickness d /mm	δ_m /mm		Error
				Experiment	Simulation	
I	8195	1500	75	23.1	23.2	0.5%
II	8195	1250	75	31.5	35.0	11.1%
III	8195	1000	75	65.2	56.8	12.9%
IV	8195	1500	0	33.7	30.7	9.0%

of slab bottom centers are presented in Table 6. It could be indicated from the results that the slab bottom displacements of the simulations agreed well with the experiment results, due to the errors below 15%.

According to the previously presented validations, the FEA model was feasible and reliable. Consequently, it could be used to analyze the dynamic response of the foam protected RC slabs under blast loads.

4. Typical event analysis

The FEA models Steel-FC-RC slabs were modeled, according to Fig. 9, to analyze the dynamic response under blast loads, marked as the basic event. The RC slabs were 3000 mm × 3000 mm × 120 mm in size. The reinforcing bars of 10 mm in diameter were spaced at 120 mm, with two-layer and two-way layouts. Also, the aforementioned clay foam ceramic was adopted as the sacrificial sandwich, of 40 mm in thickness, in the basic event.

In addition, the 2 mm thick steel plate of 235 MPa yield strength was cladded out of the foam ceramic. The weight of the charge of basic event was input as 8000 g, while the explosion distance was 1 m. The boundary conditions were set at every side of the RC slabs. In order to improve the simulation efficiency, the 1/4 modeling and the ConWep method were adopted, based on the material models.

4.1 Effective strain analysis

The cloud diagrams of foam and RC layers of effective strain were output to simulate the damage development as presented in Figs. 10-12.

Fig. 10 present the effective strain of the foam ceramic layers. As it could be observed from the diagrams, the damage of the foam ceramic expanded its areas uniformly from the center to the periphery, and as the blast effect weakened, the damage level did not increase significantly from 5.5 ms to 15 ms. Fig. 11 presents the effective strain of the top of RC slabs, while the damage mainly occurred near the supports, due to the high stress of the edges of the RC slab. 15 ms subsequently to the explosion occurrence, the central area of RC slab top begun to rebound towards the blast surface and new tensile damages occurred. Fig. 12 presents the effective strain of the RC slab bottom. It could be observed that after the slab bottom reached the peak displacement at approximately 5.5 ms, the damages in the center and diagonals stopped to expand, while a few new damages occurred near the angular points subsequently to 15 ms.

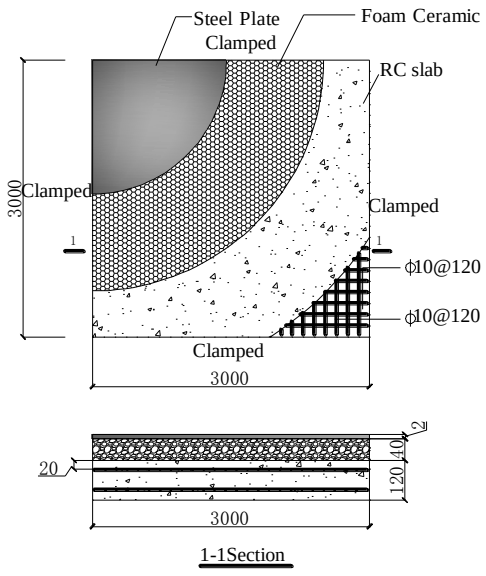

Fig. 9 Dimensions of typical blast-resistant two-way slab

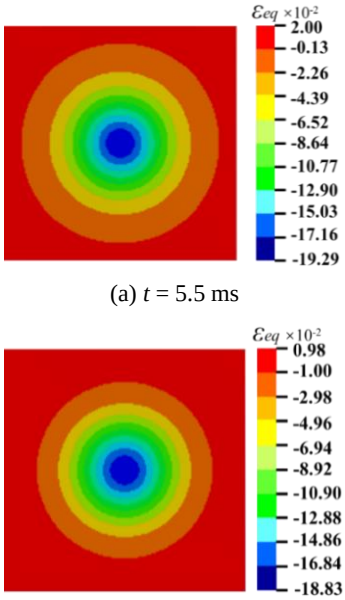

(a) t = 5.5 ms

(b) t = 15 ms

Fig. 10 Contours of effective strain of foam ceramic

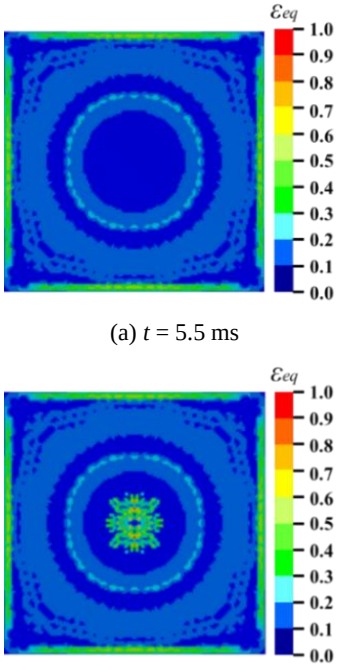

(a) t = 5.5 ms

(b) t = 15 ms

Fig. 11 Contours of effective strain of RC slab top

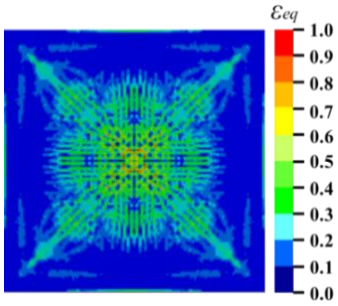

(a) t = 5.5 ms

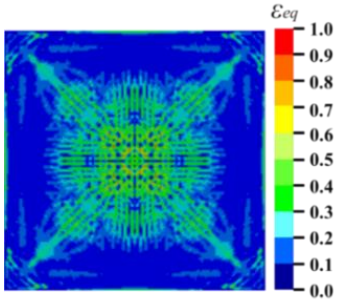

(b) t = 15 ms

Fig. 12 Contours of effective strain of RC slab bottom

4.2 Displacement analysis

The maximum displacements of the slab bottom centers were used as reference points to evaluate the damage level by previous researchers (Hou *et al.* 2018a, Nam *et al.* 2010). The displacement cloud diagrams of RC slabs at 1 ms, 5.5 ms and 15 ms are illustrated in Figs. 13-14.

For the diagrams, in which, the displacement was reduced from the edges to the center, the maximum displacement occurred at the central area of the slab bottom at 5.5 ms at 25.98 mm, while the contours of displacement transited from circle to square shapes, due to the clamped support of the edges. With the continuous reduction of the blast, the displacement decreased, while a positive rebound displacement occurred within a large area around the center point at 15 ms.

4.3 Maximum stress analysis

Since the tensile damages occurred in the areas that the stress reached the strength value, the locations of fracture damage could be predicted through the comparison between the maximum principle stress and the strength of the materials. The maximum-principle-stress (*MPS*) cloud diagrams of each layer are illustrated in Figs. 15-17.

The *MPS* in the center of foam ceramic layer was at a high level at 1.0 ms, simply after the impulse reached the blast surface, whereas the *MPS* of the RC slab was low. With the transmission of explosion waves towards the downward layer and the attenuation of the load on the blast surface, the principle stress in the central foam ceramic layer decreased, while the stress in the RC slabs and the vicinity of foam ceramic edges increased. Also, the *MPS* of RC slabs reached the peak level at 10 ms.

The *MPS* of steel plate increased gradually at a high level from 51.24 MPa (at 1 ms) to 155.45 MPa (at 10 ms), which meant that the steel plate had been left intact and reliable, before the *MPS* of RC and foam ceramic reached the peak point. At 11.8 ms, the central area of the steel plate was damaged, due to the fact that the stress exceeded the yield strength (235 MPa) and reached 284.85 MPa.

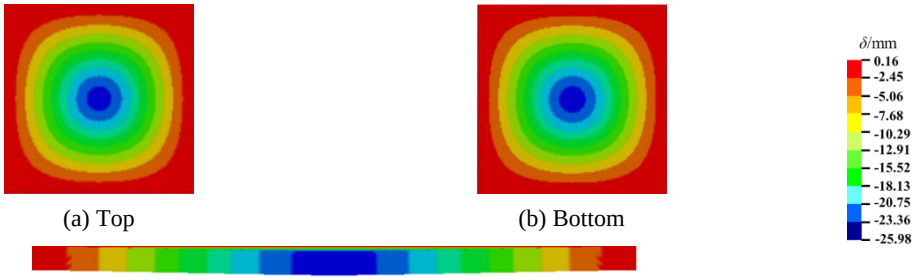

(a) Top (b) Bottom

(c) Cross section

Fig. 13 Contours of normal displacement of RC slab at t = 5.5 ms

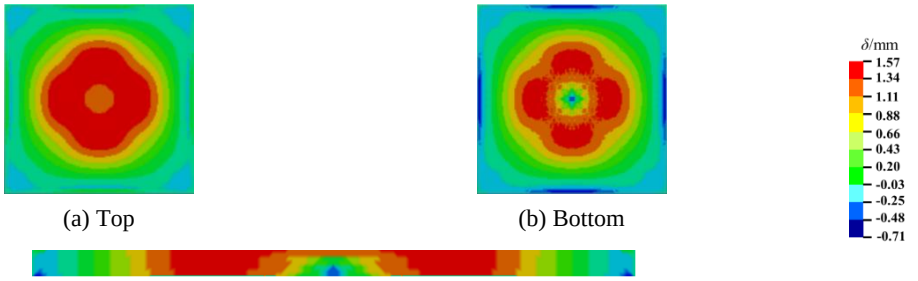

(a) Top (b) Bottom

(c) Cross section

Fig. 14 Contours of normal displacement of RC slab at t = 15 ms

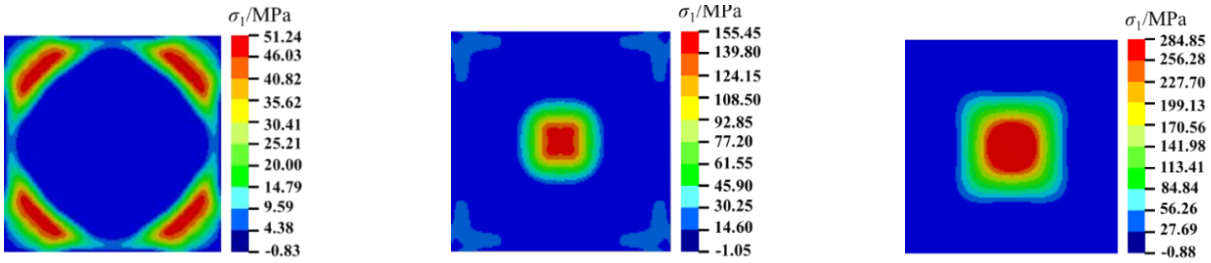

(a) t = 1 ms (b) t = 10 ms (c) t = 11.8 ms

Fig. 15 Contours of maximum principal stress of steel plate

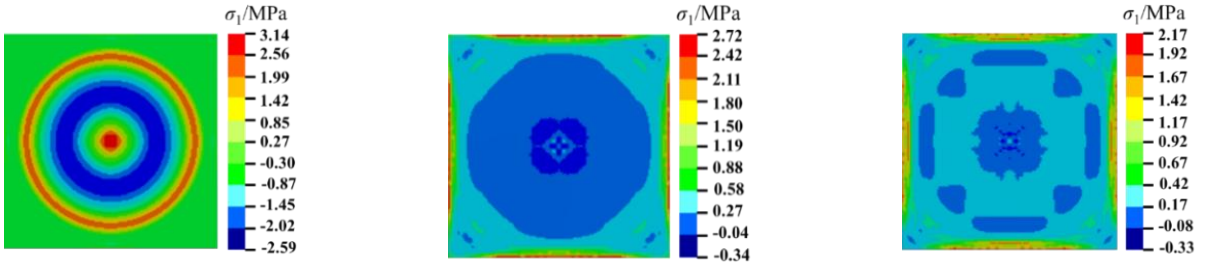

(a) t = 1 ms (b) t = 10 ms (c) t = 11.8 ms

Fig. 16 Contours of maximum principal stress of foam ceramic

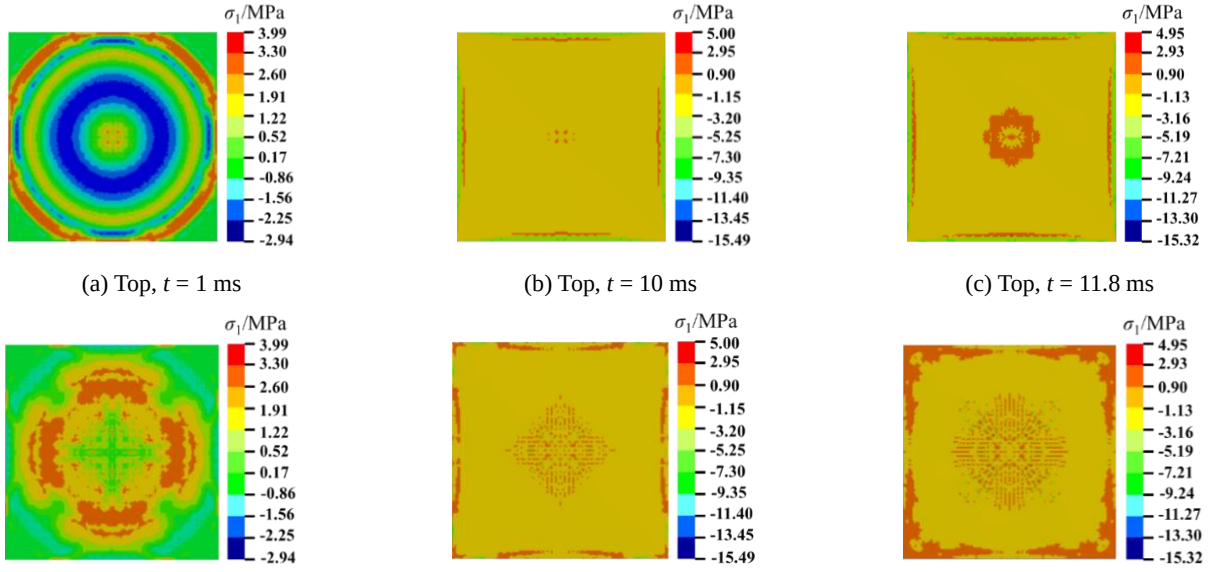

(a) Top, t = 1 ms (b) Top, t = 10 ms (c) Top, t = 11.8 ms

(d) Bottom, t =1 ms (e) Bottom, t = 10 ms (f) Bottom, t = 11.8 ms

Fig. 17 Contours of maximum principal stress of RC slaby

5. Orthogonal analysis

The analysis of dynamic response demonstrated the consistency of maximum principle stress, displacement and effective strain of the slabs. The central point displacements of the RC slabs bottom were adopted to present a reflex of the dynamic response under blast loads. Orthogonal method was adopted to analyze the influence of thickness of steel plate D_{SP}, thickness of foam ceramic layer D_{FC}, thickness of RC slab D_{RC}, compressive strength of concrete f_c and yield strength of steel bars σ_s. Besides, Appendix I provide the comparison of two different porosity of foam ceramic.

5.1 Orthogonal design and results

Based on the basic event mentioned in Section 4, an *L25* (5^6) orthogonal statistical analysis on the central bottom peak displacement was carried out under three different magnitudes of blast loads (C = 8 kg, 12 kg and 16 kg, R = 1 m), respectively.

Thickness of steel plate D_{SP}: 0, 1, 2, 3, 4 mm;

Thickness of foam ceramic layer D_{FC}: 0, 20, 40, 60, 80 mm;

Thickness of RC slab D_{RC}: 100, 120, 140, 160, 180 mm;

Compressive strength of concrete f_c: 30, 35, 40, 45, 50 MPa.

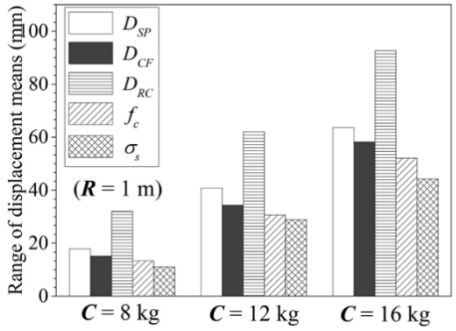

Fig. 18 Range of mean of peak displacements under three degrees of blast loads

Yield strength of steel bars σ_s: 235, 300, 400, 500, 600 MPa.

Table 7 presents the orthogonal design and its results.

5.2 Range analysis

Based on the results listed in Table 7, the means of peak displacement in each level of each factor under three different blast loads were filled and are presented in Tables 8-10, respectively (unit in the tables is mm). Consequently, the extreme differences of every column were calculated as range results. These are presented in Fig. 18. Moreover, the influence factors ranking was sorted according to the size of extreme difference of each column.

As presented in Fig. 18, the range of displacement mean of each factor increased as the blast load increased. When the D_{RC} increased from Level.1 (100 mm) to Level.5 (180 mm), the means of the peak displacement at the central bottom were reduced by 32.0 mm, 62.0 mm and 92.6 mm, under three blast loads. Moreover, for all three degrees of blast loads, the concrete slab thickness D_{RC} had the most significant influence on the displacement response among

Table 7 Orthogonal analysis results of central bottom peak displacement

Events	Factors					Central bottom peak displacement (mm)		
	D_{SP} (mm)	D_{FC} (mm)	D_{RC} (mm)	f_c (MPa)	σ_s (MPa)	C = 8 kg	C = 12 kg	C = 16 kg
OA-1	0	0	100	30	235	93.3	196.9	292.6
OA-2	0	20	120	35	300	39.3	78.7	136.3
OA-3	0	40	140	40	400	26.4	41.3	80.0
OA-4	0	60	160	45	500	17.3	25.6	45.6
OA-5	0	80	180	50	600	13.2	21.0	29.2
OA-6	1	0	120	40	500	33.4	57.7	112.7
OA-7	1	20	140	45	600	22.6	37.0	55.1
OA-8	1	40	160	50	235	15.6	24.1	45.3
OA-9	1	60	180	30	300	13.3	21.3	48.5
OA-10	1	80	100	35	400	33.1	54.9	85.9
OA-11	2	0	140	50	300	20.3	32.1	65.6
OA-12	2	20	160	30	400	21.8	34.4	90.3
OA-13	2	40	180	35	500	13.6	23.0	32.7
OA-14	2	60	100	40	600	31.3	51.1	81.2
OA-15	2	80	120	45	235	22.0	49.0	72.7
OA-16	3	0	160	35	600	16.5	27.5	54.8
OA-17	3	20	180	40	235	14.1	21.0	53.8
OA-18	3	40	100	45	300	34.5	55.4	105.0
OA-19	3	60	120	50	400	21.3	33.9	49.5
OA-20	3	80	140	30	500	17.9	29.2	47.5
OA-21	4	0	180	45	400	11.5	17.7	31.9
OA-22	4	20	100	50	500	33.5	55.8	94.6
OA-23	4	40	120	30	600	24.1	38.2	65.5
OA-24	4	60	140	35	235	17.8	28.4	42.6
OA-25	4	80	160	40	300	13.0	19.4	31.1

these factors. In addition, the priorities of influence of the factors D_{SP}, D_{FC}, f_c and σ_s sequentially decreased.

Table 8 Range analysis results for C = 8 kg, R = 1 m (unit in table: mm)

Levels	D_{SP}	D_{FC}	D_{RC}	f_c	σ_s
1	37.9	35.0	45.1	34.1	32.6
2	23.6	26.3	28.0	24.0	24.1
3	21.8	22.8	21.0	23.6	22.8
4	20.8	20.2	16.8	21.6	23.2
5	20.0	19.8	13.2	20.8	21.5
Range	17.9	15.2	32.0	13.3	11.1
Influence factor ranking	$D_{RC} > D_{SP} > D_{FC} > fc > \sigma_s$				

5.3 Trend analysis

Due to economic reasons and structural design under normal loads, the level of the aforementioned factors could not often be increased blindly. Trending analysis (presented in Fig. 19) could produce the efficiency of each factor to rationalize the selection of these factors.

It could be observed from Fig. 19 that increasing the level of each factor could weaken the displacement responses. For all factors, the efficiency of the displacement response reduction from the first level to the second level was the highest. As each factor increased to higher levels, the decreasing rate of the displacement is generally decreased.

Adversely, when C = 16 kg, R = 1 m, the D_{FC} reached 60 mm and still had high displacement reduction efficiency. The quantities of energy that the foam absorbed were roughly the same when the foam layer mass was certain.

Table 9 Range analysis results for C = 12 kg, R = 1 m (unit in table: mm)

Levels	D_{SP}	D_{FC}	D_{RC}	f_c	σ_s
1	72.7	66.4	82.8	64.0	63.9
2	39.0	45.4	51.5	42.5	41.4
3	37.9	36.4	33.6	38.1	36.4
4	33.4	32.0	26.2	36.9	38.3
5	31.9	34.7	20.8	33.4	35.0
Range	40.8	34.4	62.0	30.6	28.9
Influence factor ranking	$D_{RC} > D_{SP} > D_{FC} > fc > \sigma_s$				

Table 10 Range analysis results for C = 16 kg, R = 1 m (unit in table: mm)

Levels	D_{SP}	D_{FC}	D_{RC}	f_c	σ_s
1	116.8	111.5	131.9	108.9	101.4
2	69.5	86.0	87.3	70.5	77.3
3	68.5	65.7	58.1	71.8	67.5
4	62.1	53.5	53.4	62.0	66.6
5	53.1	53.3	39.2	56.8	57.2
Range	63.7	58.2	92.6	52.1	44.2
Influence factor ranking	$D_{RC} > D_{SP} > D_{FC} > fc > \sigma_s$				

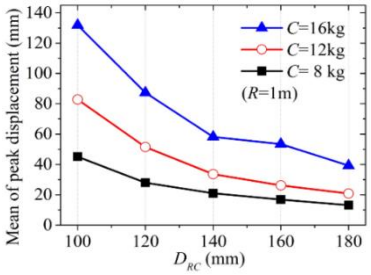

(a) Thickness of RC slab D_{RC}

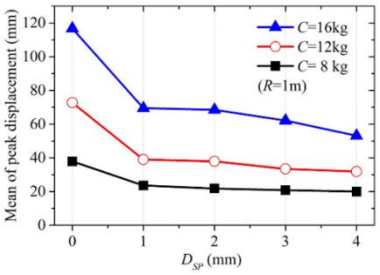

(b) Thickness of steel plate D_{SP}

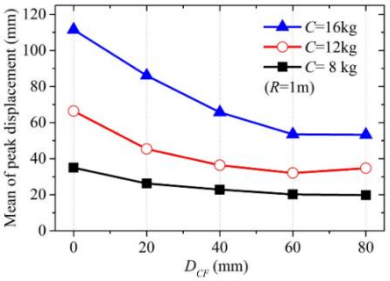

(c) Thickness of foam ceramic D_{FC}

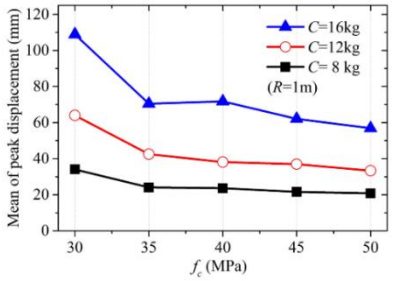

(d) Compressive strength of concrete f_c

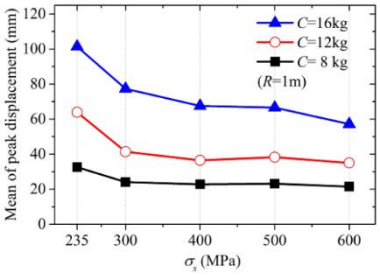

(e) Yield strength of steel bars σ_s

Fig. 19 Trend chart of each factor on mean of peak displacement

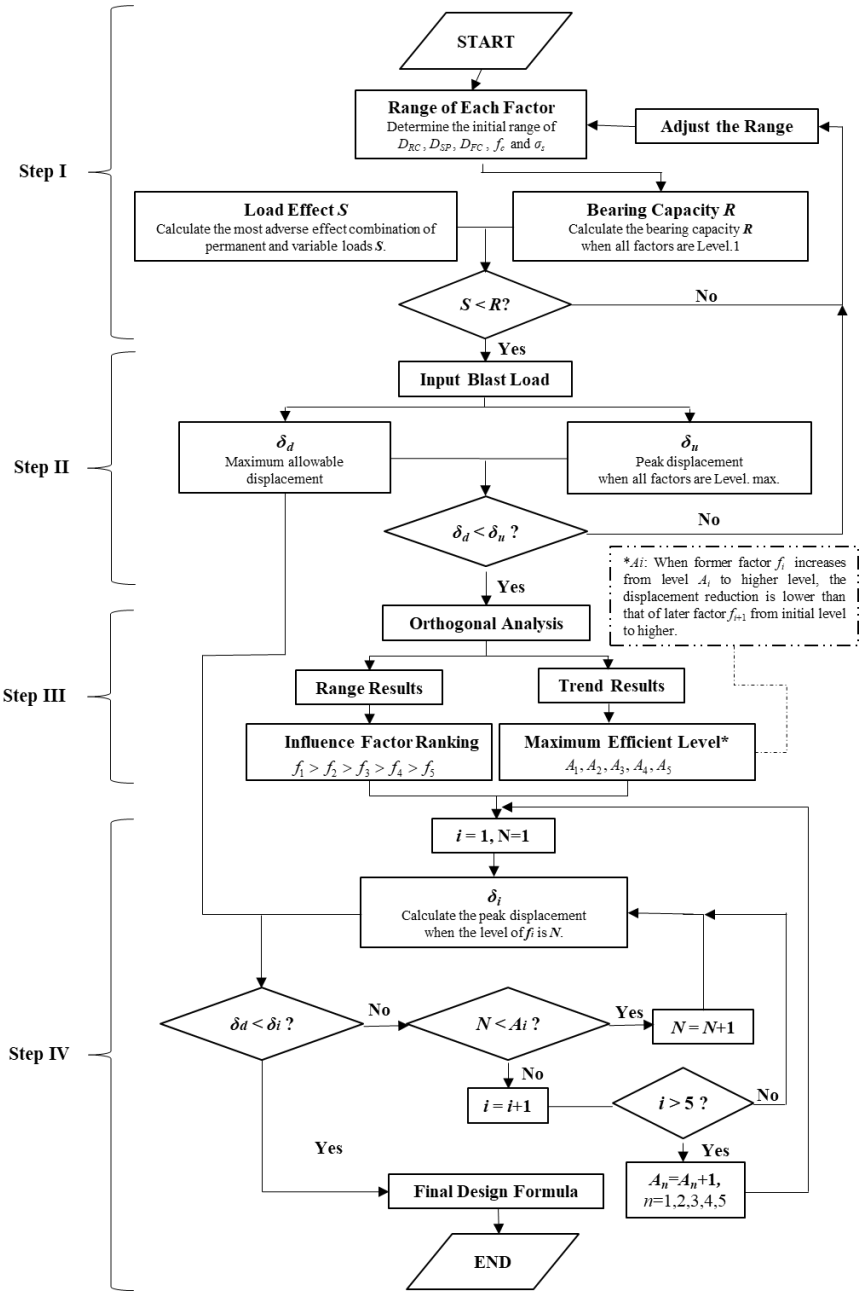

Fig. 20 Flow chart of efficient design method of steel-foam ceramic protected RC slabs

This signified that the thicker foam layers displayed higher upper limit of energy absorption. Therefore, as long as the blast load was sufficiently high, exceeding the energy that the foam could absorb, the D_{FC} increase was still an effective way to weaken the displacement responses.

According to the analysis, it was recommended to determine the values of each factor in the order of influence ranking ($D_{RC} > D_{SP} > D_{FC} > f_c > \sigma_s$).

An efficient design method was proposed based on the orthogonal analysis, consisting of four steps (presented in Fig. 20):

Step I: Determination of the initial range of the factors, and check whether the slab with factors of lowest levels could meet the bearing capacity requirements under permanent and variable loads or not.

Step II: Verification of whether the slabs with factors of maximum levels could meet the displacement requirements under blast loads or not.

Step III: Obtaining the influence factor ranking and maximum efficient level of each factor through the orthogonal analysis.

Step IV: Changing the level of each factor sequentially in the order of the influence ranking. When the former factor reaches the maximum efficient level, then consider changing the later factors. Following this practice, the efficient design could be obtained as final formula of each factor.

Considering C = 16 kg (R = 1 m) as an example. For factor D_{RC}, D_{RC} = 140 mm was selected, due to the relatively lower reduction rate of displacement when D_{RC} >

140 mm. If a higher anti-explosion requirement existed for the slabs or a structural limit on D_{RC}, the addition of a 1mm steel plate would be the most efficient method. If the requirement was further raised, the D_{FC} would be considered to be increased until D_{FC} = 60 mm. Similarly, when D_{FC} = 60 mm the requirement could still not be met. In this case, it would be useful to increase the fc to 35 MPa or the σs to 300 MPa.

6. Conclusions

The following conclusions could be drawn:

- Dynamic response of Steel-FC-RC slabs under blast loading was preliminarily studied by numerical simulations.
- The dynamic displacement of the slab bottom was significantly reduced by increasing the thickness of steel plate, foam ceramic and RC slab, while the displacement decreased slightly as the steel yield strength and the compressive strength of concrete increased. However, the optimized efficiency of blast resistance decreases with factors increase to higher level.
- Based on the orthogonal analysis and within the range of factors stated in 6.1, the influence factor ranking under three degree of blast load (C = 8, 12 and 16 kg, R = 1 m) was obtained: $D_{RC} > D_{SP} > D_{FC} > fc > \sigma_s$. Besides, the Steel-FC-RC slabs could be designed effectively and efficiently following the influence factor ranking order.

Acknowledgments

The study presented in this paper, is supported by the National Natural Science Foundation of China (No. 51578184, No. 51408167), Excellent Youth Science Foundation of Heilongjiang Province (No. YQ2019E028), Natural Science Foundation of the Heilongjiang Province (QC2017058), and Heilongjiang Youth Innovative Talent Training Program (UNPYSCT-2017085).

References

Abid, M., Hou, X., Zheng, W. and Hussain, R.R. (2019), "Effect of fibers on high-temperature mechanical behavior and microstructure of reactive powder concrete", *Materials*, **12**(2), 329. https://doi.org/10.3390/ma12020329

Castedo, R., Segarra, P., Alanon, A., Lopez, L.M., Santos, A.P. and Sanchidrian, J.A. (2015), "Air blast resistance of full-scale slabs with different compositions: Numerical modeling and field validation", *Int. J. Impact Eng.*, **86**, 145-156. https://doi.org/10.1016/j.ijimpeng.2015.08.004

Chen, X., Chen, C., Xu, L. and Shao, Y. (2016), "Dynamic flexural strength of concrete under high strain rates", *Magaz. Concrete Res.*, **69**(3), 109-119. https://doi.org/10.1680/jmacr.15.00548

Chen, X., Ge, L., Zhou, J. and Wu, S. (2017), "Dynamic Brazilian test of concrete using split Hopkinson pressure bar", *Mater. Struct.*, **50**(1), 1-10. https://doi.org/10.1617/s11527-016-0885-6

Chuda-Kowalska, M. and Garstecki, A. (2016), "Experimental study of anisotropic behavior of PU foam used in sandwich panels", *Steel Compos. Struct., Int. J.*, **20**(1), 43-56. https://doi.org/10.12989/scs.2016.20.1.043

Codina, R., Ambrosini, D. and de Borbón, F. (2017), "New sacrificial cladding system for the reduction of blast damage in reinforced concrete structures", *Int. J. Protect. Struct.*, **8**(2), 221-236. https://doi.org/10.1177/2041419617701571

CYMAT (2008), Technical Manual for CYMAT, CYMAT Group, Canada.

Dear, J.P., Rolfe, E., Kelly, M., Arora, H. and Hooper, P.A. (2017), "Blast performance of composite sandwich structures", *Procedia Eng.*, **173**, 471-478. https://doi.org/10.1016/j.proeng.2016.12.065

Foglar, M., Hajek, R., Fladr, J., Pachman, J. and Stoller, J. (2017), "Full-scale experimental testing of the blast resistance of HPFRC and UHPFRC bridge decks", *Constr. Build. Mater.*, **145**, 588-601. https://doi.org/10.1016/j.conbuildmat.2017.04.054

Guzas, E.L. and Earls, C.J. (2010), "Air blast load generation for simulating structural response", *Steel Compos. Struct., Int. J.*, **10**(5), 429-455. https://doi.org/10.12989/scs.2010.10.5.429

Hafizi, M.N., Risby, M.S., Umar, S.T., Isa, M.F.M., Sohaimi, A.S.M. and Khalis, S. (2017), "Experimental and numerical investigation on blast wave propagation in soil structure", *J. Fundam. Appl. Sci.*, **9**(3S), 221-230. http://dx.doi.org/10.4314/jfas.v9i3s.19

Hanssen, A.G., Enstock, L. and Langseth, M. (2002), "Close-range blast loading of aluminum foam panels", *Int. J. Impact Eng.*, **27**(6), 593-618. https://doi.org/10.1016/S0734-743X(01)00155-5

Hao, H., Hao, Y., Li, J. and Chen, W. (2016), "Review of the current practices in blast-resistant analysis and design of concrete structures", *Adv. Struct. Eng.*, **19**(8), 1193-1223. https://doi.org/10.1177/1369433216656430

Hou, X., Cao, S., Rong, Q. and Zheng, W. (2018a), "A P-I diagram approach for predicting failure modes of RPC one-way slabs subjected to blast loading", *Int. J. Impact Eng.*, **120**, 171-184. https://doi.org/10.1016/j.ijimpeng.2018.06.006

Hou, X., Cao, S., Rong, Q., Zheng, W. and Li, G. (2018b), "Effects of steel fiber and strain rate on the dynamic compressive stress-strain relationship in reactive powder concrete", *Constr. Build. Mater.*, **170**, 570-581. https://doi.org/10.1016/j.conbuildmat.2018.03.101

Hou, X., Cao, S., Rong, Q., Zheng, W. and Li, G. (2018c), "Experimental study on dynamic compressive properties of fiber-reinforced reactive powder concrete at high strain rates", *Eng. Struct.*, **169**, 119-130. https://doi.org/10.1016/j.engstruct.2018.05.036

Hou, X., Ren, P. and Rong, Q. (2019), "Effect of fire insulation on fire resistance of hybrid-fiber reinforced reactive powder concrete beams", *Compos. Struct.*, **209**, 219-232. https://doi.org/10.1016/j.compstruct.2018.10.073

Jayasooriya, R., Thambiratnam, P.D. and Perera, J.N. (2014), "Blast response and safety evaluation of a composite column for use as key element in structural systems", *Eng. Struct.*, **61**, 31-43. https://doi.org/10.1016/j.engstruct.2014.01.007

Jing, L., Wang, Z. and Zhao, L. (2013), "Dynamic response of cylindrical sandwich shells with metallic foam cores under blast loading—Numerical simulations", *Compos. Struct.*, **99**(5), 213-223. https://doi.org/10.1016/j.compstruct.2012.12.013

Kodur, V. (2014), "Properties of concrete at elevated temperatures", *ISRN Civil Engineering*, **2014**,1-15. http://dx.doi.org/10.1155/2014/468510

Krundaeva, A., De Bruyne, G., Gagliardi, F. and Van Paepegem, W. (2016), "Dynamic compressive strength and crushing properties of expanded polystyrene foam for different strain rates and different temperatures", *Polym. Test.*, **55**, 61-68.

https://doi.org/10.1016/j.polymertesting.2016.08.005
Langdon, G.S., Von Klemperer, C.J., Rowland, B.K. and Nurick, G.N. (2012), "The response of sandwich structures with composite face sheets and polymer foam cores to air-blast loading: preliminary experiments", *Eng. Struct.*, **36**, 104-112. https://doi.org/10.1016/j.engstruct.2011.11.023
Li, S., Li, N. and Li, Y. (2008), "Processing and microstructure characterization of porous corundum–spinel ceramics prepared by in situ decomposition pore-forming technique", *Ceram. Int.*, **34**(5), 1241-1246. https://doi.org/10.1016/j.ceramint.2007.03.018
Li, X., Huang, R., Li, Y. and Gao, G. (2013), "Experimental research of foamed ceramic composite under dynamic loading using SHPB", *Adv. Mater. Res.*, **718-720**, 112-116. https://doi.org/10.4028/www.scientific.net/AMR.718-720.112
Liang, M., Lu, F., Zhang, G. and Li, X. (2017), "Design of stepwise foam claddings subjected to air-blast based on Voronoi model", *Steel Compos. Struct., Int. J.*, **23**(1), 107-114. https://doi.org/10.12989/scs.2017.23.1.107
Luo, W. (2011), "Study on mechanical properties of ceramic foams and application in defense works", Master's Dissertation; University of Science and Technology of China, Hefei, China. [In Chinese]
Luo, T. (2015), "Study on the Preparation Process and Anti-ballistic Properties of Ceramic Composite Targets Confined by Fiber", Master's Dissertation; Beijing Institute of Technology, Beijing, China, pp. 26-27. [In Chinese]
LS-DYNA (2006), Keyword user's manual Livermore, Livermore Software Technology Corporation, CA, USA.
Mehr, M., Davis, C., Sadman, K., Hooper, R.J., Manuel, M.V. and Nino, J.C. (2016). "Epoxy interface method enables enhanced compressive testing of highly porous and brittle materials", *Ceram. Int.*, **42**(1), 1150-1159. https://doi.org/10.1016/j.ceramint.2015.09.045
Mondal, D.P., Jha, N., Badkul, A., Das, S. and Khedle, R. (2012), "High temperature compressive deformation behaviour of aluminum syntactic foam", *Mater. Sci. Eng.: A*, **534**, 521-529. https://doi.org/10.1016/j.msea.2011.12.002
Murray, Y.D., Abu-Odeh, A.Y. and Bligh, R.P. (2007), "Evaluation of LS-DYNA concrete material model 159", No. FHWA-HRT-05-063; Department of Transportation, USA.
Nam, J.W., Kim, H.J., Kim, S.B., Yi, N.H. and Kim, J.H.J. (2010), "Numerical evaluation of the retrofit effectiveness for GFRP retrofitted concrete slab subjected to blast pressure", *Compos. Struct.*, **92**(5), 1212-1222. https://doi.org/10.1016/j.compstruct.2009.10.031
Nie, B., He, X., Zhang, R., Chen, W. and Zhang, J. (2011), "The roles of foam ceramics in suppression of gas explosion overpressure and quenching of flame propagation", *J. Hazard. Mater.*, **192**(2), 741-747. https://doi.org/10.1016/j.jhazmat.2011.05.083
Ousji, H., Belkassem, B., Louar, M.A., Reymen, B., Pyl, L. and Vantomme, J. (2016), "Experimental study of the effectiveness of sacrificial cladding using polymeric foams as crushable core with a simply supported steel beam", *Adv. Civil Eng.*, **2016**, 1-13. http://dx.doi.org/10.1155/2016/8301517
Pham, T. M., Chen, W., Kingston, J. and Hao, H. (2018), "Impact response and energy absorption of single phase syntactic foam", *Compos. Part B: Eng.*, **150**, 226-233. https://doi.org/10.1016/j.compositesb.2018.05.057
Pinnoji, P.K., Mahajan, P. and Bourdet, N. (2010), "Impact dynamics of metal foam shells for motorcycle helmets: Experiments & numerical modeling", *Int. J. Impact Eng.*, **37**(3), 274-284. https://doi.org/10.1016/j.ijimpeng.2009.05.013
Rashad, M. and Yang, T.Y. (2018), "Numerical study of steel sandwich plates with RPF and VR cores materials under free air blast loads", *Steel Compos. Struct., Int. J.*, **27**(6), 717-725. https://doi.org/10.12989/scs.2018.27.6.717
Shi, D. and Chen, X. (2018), "Flexural Tensile Fracture Behavior of Pervious Concrete under Static Preloading", *J. Mater. Civil Eng.*, **30**(11), 06018015-1-7. https://doi.org/10.1061/(ASCE)MT.1943-5533.0002477
Silva, B.B.R., Santana, R.M.C and Forte, M.M.C. (2010), "A solventless castor oil-based PU adhesive for wood and foam substrates", *Int. J. Adhes. Adhes.*, **30**(7), 559-565. https://doi.org/10.1016/j.ijadhadh.2010.07.001
Wei, C., Xu, M., Sun, J., Fan, H. and Xie, S. (2011) "Design and mechanics analysis of explosive-barrier devices in mining face based on ceramic foam", *Proceedings of the 2nd International Conference on Artificial Intelligence, Management Science & Electronic Commerce*, pp. 1050-1053. https://doi.org/10.1109/AIMSEC.2011.6010684
Wu, C., Huang, L. and Oehlers, D.J. (2011), "Blast testing of aluminum foam-protected reinforced concrete slabs", *J. Perform. Constr. Facil.*, **25**(5), 464-474. https://doi.org/10.1061/(ASCE)CF.1943-5509.0000163
Xia, Y., Wu, C., Zhang, F., Li, Z.X. and Bennett, T. (2014), "Numerical analysis of foam-protected RC members under blast load", *Int. J. Protect. Struct.*, **5**(4), 367-390. https://doi.org/10.1260/2041-4196.5.4.367
Xia, Y., Wu, C., Liu, Z.X. and Yuan, Y. (2016), "Protective effect of graded density aluminum foam on RC slab under blast loading–An experimental study", *Constr. Build. Mater.*, **111**, 209-222. https://doi.org/10.1016/j.conbuildmat.2016.02.092
Xu, J. and Lu, Y. (2013), "A comparative study of modelling RC slab response to blast loading with two typical concrete material models", *Int. J. Protect. Struct.*, **4**(3), 415-432. https://doi.org/10.1260/2041-4196.4.3.415
Ye, Z.B., Li, Y.C., Zhao, K., Huang, R.Y., Zhang, Y.L. and Sun, X.W. (2018), "New form of equivalent constitutive model for combined shell particle composites and its application in civil air defense", *Int. J. Civil Eng.*, **17**(5), 555-561. https://doi.org/10.1007/s40999-018-0324-x
Zake-Tiluga, I., Svinka, V., Svinka, R. and Grase, L. (2015). "Thermal shock resistance of porous Al_2O_3-mullite ceramics", *Ceram. Int.*, **41**(9), 11504-11509. https://doi.org/10.1016/j.ceramint.2015.05.116
Zhang, J.F., Liang, X.M., Ma, Z.Y., Yang, Y.Y., Liang, J.J., Zhu, H.Y., Wang, T.W. and Wang, S.J. (2011), "Study on chain scission of gas explosion reaction in foam ceramics", *Procedia Eng.*, **26**, 2369-2375. https://doi.org/10.1016/j.proeng.2011.11.2447
Zhou, D., Li, R., Wang, J. and Guo, C. (2017), "Study on Impact Behavior and Impact Force of Bridge Pier Subjected to Vehicle Collision", *Shock Vib.*, **2017**, 1-12. https://doi.org/10.1155/2017/7085392
Zhu, C., Lin, Z.T.L., Chia, Y.F. and Chong, K.P. (2009), "Protection of reinforced concrete structures against blast loading", Final Year Research Project Report; The University of Adelaide, Adelaide, Australia.

CC

Appendix I

Foam ceramics with different porosities have different dynamic compressive strength, different density and different stress-strain curves (Luo 2011). In order to analyze the porosity influence of foam ceramic on displacement responses, based on the basic event, two different porosities (64% and 45%) were studied for two different events: C = 8 kg and C = 16 kg (R = 1 m).

The parameters of 64% foam ceramic porosity are presented in Table 11, while the parameters of 45% foam ceramic porosity were previously mentioned in section 2.1. In addition, the stress-strain curves of the foam ceramic with two different porosities are presented in Fig. 21.

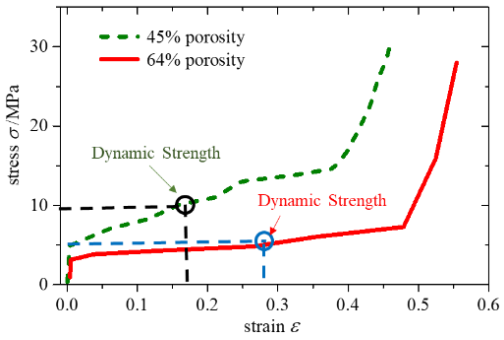

Fig. 21 Stress-strain curves of foam ceramic with two different porosities

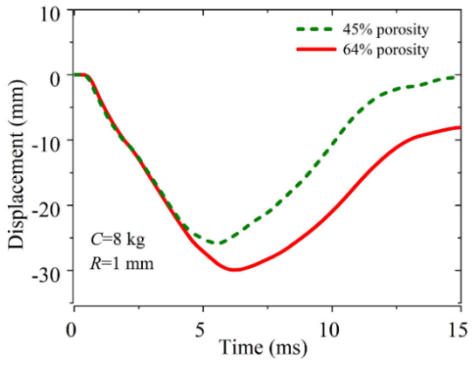

(a) C = 8 kg, R = 1 m

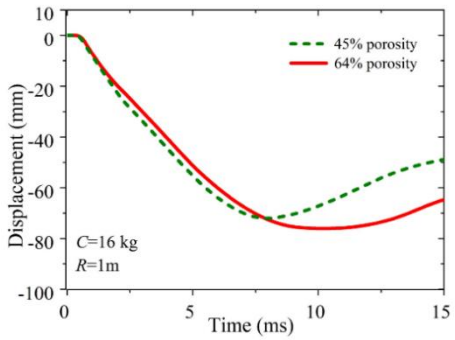

(b) C= 16 kg, R = 1 m

Fig. 22 Displacement time history curves of central points with different porosities of foam ceramic

The displacement results illustrated in Figs. 22 demonstrated that, at lower blast load level, as an example, C = 8 kg and R = 1000 mm, the foam ceramic with lower porosity was more capable of reducing the displacement response, while the peak displacement was reduced by 13.60%. Also, at higher blast load event, such as C = 16 kg and R = 1 m, the difference between these two foam ceramics was only 5.27%.

The reason was that, although these two foam ceramics presented different stress-strain curves, the maximum energy that could be absorbed was cut off at an equivalent dynamic strength. The maximum energy absorption per volume E_m could be calculated as follows

$$E_m = \int_0^{\varepsilon_D} \sigma d\varepsilon \tag{4}$$

The difference of E_m between the two different foam ceramics was only 13.3% (listed in Table 12). Therefore, it could be concluded that, different foam ceramics presented different stress-strain curves and dynamic strength, while these two parameters were closely related to the energy absorption effect, consequently affecting the dynamic response of the slabs.

Table 11 Parameters of foam ceramic of 0.64 and 0.45 porosity

Parameter	Density /(kg/m^3)	Poisson ratio	Modulus of elasticity /MPa	Dynamic strength /MPa	Stress-strain curve
Value	620	0.108	810	5.01	Fig. 21
Value	930	0.114	1192	9.41	Fig. 21

Table 12 Peak displacements of central points with different foam porosities at different events

Porosity	Peak displacements (mm) (C = 8 kg, R = 1000 mm)	Peak displacements (mm) (C = 16 kg, R = 1000 mm)	E_m (MPa)
64%	29.9	76.1	1.1
45%	25.9	72.0	1.3
Difference	13.6%	5.3%	-13.3%